Benajes, J.; Novella Rosa, R.; Gómez-Soriano, J.; Barbery-Avila, II.; Libert, C. (2021). Advantages of hydrogen addition in a passive pre-chamber ignited SI engine for passenger car applications. International Journal of Energy Research. 45(9):13219-13237. https://doi.org/10.1002/er.6648

Advantages of hydrogen addition in a passive pre-chamber ignited SI engine for passenger car applications

J. Benajes[a], R. Novella[a], J. Gomez-Soriano[a,*], I. Barbery[a], C. Libert[b]

[a]*CMT – Motores Térmicos, Universitat Politècnica de València, Camino de Vera, 46022 Valencia, Spain*
[b]*DEA-IRP Groupe Renault, 1 avenue du Golf. 78084, Guyancourt, France*

Abstract

Hydrogen is one of the most promising alternative fuels for the transportation industry. The use of hydrogen to enable lean burn in internal combustion engines is an attractive solution for reducing CO_2 emissions from two points of views: the substitution of carbon-based fuels and the increased thermal efficiency due to lean operation. Combining this strategy with the passive pre-chamber ignition system with gasoline/hydrogen blends, is even more interesting. The main limitations of the passive pre-chamber concept in a high compression ratio spark-ignition engine were shown through engine experiments. A numerical study was then performed to evaluate the chance of extending the dilution limit by using hydrogen along with this technology. Results show how the use of hydrogen provides considerable benefits in the main chamber combustion process by enhancing the thermo-chemical properties of the mixture, increasing the flame speed and improving the flame structure. Using an adequate gasoline-hydrogen blend proved to enable optimum burning rates at lean conditions leading to a relevant thermal efficiency gain.

Keywords: *Hydrogen combustion, spark-ignition engine, passive pre-chamber, ultra-lean combustion, Computational Fluid Dynamics*

1. Introduction

Every year the energy crisis associated with the world's demand of natural resources, used to power the industrial infrastructure of society, is becoming more urgent [1]. As human population grows, so does the consumption of energy coming from the limited fossil fuels that are available in the planet. Additionally, burning these fuels contributes to the production of Green House Gases (GHG) like Carbon Dioxide (CO_2), Hydro-Carbon (HC) and other air-polluting emissions. These facts motivated several global treaties based on multiple research works, such as the Paris Agreement [2], to aim for a decarbonization of the global energy network to improve sustainability and reduce pollution.

This goal can be achieved by the implementation of renewable energy resources [3], which in terms of production and infrastructure is still being widely investigated and developed in order to be sustainable in the current global economy. However, another way of achieving this goal is by the use of alternative fuels. Among these fuels, hydrogen (H_2) arises as a promising energy source for the future industry [4].

In the transportation sector, there is currently a broad discussion about the future of this particular fuel, whether it should be used in Internal Combustion Engines (ICE) or in Fuel Cell Vehicles (FCV) is a hot topic of debate [5]. Near future prospects show that customer requirements will be better met by Hydrogen Internal Combustion Engines (H_2ICE) rather than FCV's [6], considering that the FCV's infrastructure (hydrogen storage, production, transportation and distribution means) is still in the early phase of implementation.

As a fuel, hydrogen has many advantages that are unmatched by any other alternative fuel candidate. It is the most abundant and lightest element in the universe, that can be synthesized or produced by multiple processes. For example, hydrogen is widely produced by burning natural gas in the modern industry. But other cleaner alternative processes such as photovoltaic, wind or even geothermal [7, 8], are currently being implemented for producing this fuel in large scales.

Hydrogen has a high energy content (Lower heating value), being almost three times higher than gasoline fuel. In terms of combustion, hydrogen shows numerous benefits such as high reactivity, diffusivity, and flammability which entails elevated burning rates. In addition to these interesting properties, combustion products of hydrogen oxidation do not contain any carbon-based elements. Thus, hydrogen will contribute to reduce the environmental footprint of transportation by avoiding both hydrocarbon and CO_2 emissions [9].

However, the low energy density of hydrogen combined with store-related issues are two of the main limitations of this technology [10]. For this reason several efforts are being devoted to combine this strategy with dual fuel blends, such as diesel or gasoline surrogates [11, 12], to reduce the amount of hydrogen required for the vehicle operation, thereby solving both issues.

*Corresponding author.
Tel.: +34 96 387 70 00 (ext. 76537), fax: +34 96 387 76 59
email: jogoso1@mot.upv.es

Recent trends indicate that spark-ignition (SI) engines are currently the main powerplant for passenger cars, having replaced compression-ignition (CI) engines due to the highly expensive aftertreatment systems required to fulfill the stringent air polluting standards of modern society [13]. However, SI engines are very limited in efficiency as knocking combustion compromises the integrity of the engine [14] and forbids the use of higher compression ratios [15]. Moreover, SI engines must be operated in stoichiometric conditions for compatibility with the state-of-the-art Three-Way Catalyst (TWC) technology [16] used to control tailpipe Nitrogen Oxides (NO_x) emissions, further limiting the engine thermal efficiency.

In view of this, modern eco-friendly engine cycles [17] and several strategies [18] are currently the focus of many investigations aiming towards improving the thermal efficiency of SI engines. In particular, burning lean air-fuel mixtures ($\lambda > 1$) has shown an improvement of the engine efficiency in several ways [19, 20], reducing the CO_2 generation for the same amount of energy. Nevertheless, using lean mixtures to operate SI engines also entails some drawbacks. Mainly, the flame propagation speed decreases as the air-to-fuel ratio (λ) increases, which leads to incomplete combustion, misfires and high cycle-to-cycle variability (CCV), compromising the performance of the engine. Additionally, this strategy is not compatible with the TWC and elevated dilution levels ($\lambda > 1.8$) are required to fulfill the emissions standards. Such elevated λ values reduce combustion temperatures well below 1800K, thus preventing the formation of NO_x as the activation energy for nitrogen oxidation is not reached [21].

Therefore, the use of a gasoline/hydrogen blend can be an interesting solution for overcoming these limitations as the combustion velocities increase significantly and the flame should be able to propagate adequately in an extremely lean environment. This hypothesis was confirmed by Li et al. [22] and Ilbas et al. [23], whom studied the effects of hydrogen enrichment on ammonia-based and methane-based fuels in small burners. Moreover, Hamori et al. [24] and Toulson et al. [25] verified that the burning λ limit for a hydrogen combustion in ICE is significantly higher than a conventional ICE operating with gasoline. Although there are multiple breakthroughs in the understanding of combustion characteristics of hydrogen enriched flames in multiple research devices, the applicability of this knowledge is still in its early stage. While there are plenty of research works related to constant-volume chambers [26, 27], scaled burners [28] or rapid compression machines [29]; the state-of-the-art in H_2 ICE is more limited and mostly focused on developing engines fueled by pure hydrogen [30]. Nonetheless, this approach is still difficult to implement for commercial transportation in passenger cars due to severe economic constraints.

The pre-chamber ignition system [31], or Turbulent Jet Ignition (TJI), being widely established in high-power stationary powerplants [32], is also an interesting technology to incorporate in future SI engines. This ignition strategy uses a standard spark plug to initiate combustion in a small volume "pre-chamber", which is connected to the main combustion chamber through one or several small holes [33]. In engine applications, due to spatial limitations, the pre-chamber volume is usually between 2% and 5% of the clearance volume at Top Dead Center [19]. Several studies [34, 35, 36] have highlighted the benefits of the TJI concept for mitigating knocking combustion, reducing CCV and improving other negative effects associated to lean combustion in SI engines.

Two approaches can be used for implementing the pre-chamber ignition concept. The first approach consists in installing a dedicated injector inside the pre-chamber, thereby directly controlling the air-to-fuel ratio in this region independently from the main chamber charge. This is called an active system, and allows to operate the pre-chamber at stoichiometric conditions for optimum burning rates [37]. This concept is compatible with the use of hydrogen fuel and it has been studied since 1992 as a potential combustion strategy called Hydrogen Assisted Jet Ignition (HAJI) [38, 39], for igniting H_2-enriched mixtures inside the pre-chamber. Nevertheless, the pre-chamber injector is complicated and expensive to manufacture.

The second approach is known as a passive system, where no auxiliary fuel is supplied into the pre-chamber, thus its air-to-fuel ratio is controlled by the main injection system [40]. In Port Fuel Injection (PFI) engines, both combustion chambers essentially share the same mixture composition, causing the ignition and propagation issues found in conventional SI operation to be transferred to the pre-chamber when diluting the mixture. However, since packaging and installation are fairly simple for implementing this approach, no relevant engine modifications are required.

This paper presents an evaluation of a feasible short-term solution for implementing hydrogen fuel in modern SI engines by combining the passive pre-chamber ignition system with a premixed gasoline/hydrogen blend injected in the intake port. Through this approach, other interesting strategies such as lean combustion can be enabled for improving the thermal efficiency and fuel consumption with the inherent reduction of CO_2 emission and pollutants. In this sense, the issue of CO_2 emissions is addressed though two different, but closely related, paths: the substitution of carbon-based fuels and the increased thermal efficiency due to lean operation.

Therefore, an innovative numerical methodology is developed for evaluating the integration of the passive pre-chamber ignition system with hydrogen enriched fuel blends in a representative passenger car engine. From an analysis of the mixture laminar flame speed by 1D chemical simulations to detailed 3D Computational Fluid Dynamics (CFD) simulations, this combustion concept is deeply evaluated under realistic engine conditions. In particular, the basis and understanding of the pre and main chamber combustion features when operating at lean conditions are addressed. Different concentrations of hydrogen are simulated at constant energy conditions to isolate the effects of H_2 addition over the combustion process itself. Finally, the potential benefits that this integrated solution brings over the engine indicated efficiency and NO_x formation are highlighted.

Table 1: *Main features of the engine.*

Engine	4-stroke SI
Number of cylinders [-]	1
Displacement [cm^3]	404
Bore – Stroke [mm]	80.0 – 80.5
Compression ratio (geometric) [-]	13.4:1
Valvetrain [-]	DOHC
Number of valves/cylinder [-]	2 intake and 2 exhaust
Fuel injection system [-]	PFI (p_{max} = 6 bar)

2. Tools and methodology

A computational study was performed using 3D-CFD simulations of a turbocharged SI engine, equipped with a pre-chamber ignition system. The numerical simulations were previously validated with results from an experimental campaign performed in the engine, both at stoichiometric conditions and at the measured air-dilution limit. Thereafter, simulations were carried out for extending the mixture dilution beyond the limit with the help of H_2 addition.

2.1. Engine characteristics and test-bench

The experimental campaign was performed in a single-cylinder research version of a 4-stroke turbocharged SI engine, fueled with 95 Research Octane Number (RON95) gasoline injected in the intake port (PFI). The injection system was installed 270 mm away from the cylinder head block in order to ensure the homogeneity of the air-fuel mixture. This strategy allowed fair analysis of pre-chamber initiated combustion while diminishing other side effects related to the mixture stratification that can condition the combustion process in a significant way. A high compression ratio (13.4:1) was used considering that the pre-chamber ignition system helps to mitigate knocking appearance by rising the burning rate in the main combustion chamber. A summary of the engine characteristics is shown in Table 1.

The engine was assembled into a fully instrumented test cell. Several equipment and hardware were installed to operate the engine and monitor relevant parameters such as the fuel, oil and water temperatures, pollutant emissions, fuel consumption, instantaneous pressure signals in the cylinder, intake and exhaust lines, among others. An external compressor was used for providing the compressed air, necessary to simulate boost conditions. The full details of the engine test-bench are described in [36].

The operating point for performing the experiments is shown in Table 2 and was selected based on previous studies from the authors [36, 41] as it provides the highest benefits, in terms of engine thermal efficiency. The combination of high-load and high-speed conditions (4500 rpm and 12.8 bar IMEP) is an interesting case of study considering that the pre-chamber scavenge is compromised, due to the short period of time available for the filling process and end-gas auto-ignition knocking arises due to the elevated engine load.

An in-house 0D combustion diagnosis tool was used to calculate the cycle-averaged values of combustion-related parameters such as the apparent Heat Release Rate (HRR), the combustion phasing (CA50), the indicated mean effective pressure and its variability (IMEP & σIMEP). The software uses the in-cylinder pressure signal from the experiments to estimate the heat release from combustion by solving the energy equation assuming several simplifications and isolating the heat transfer losses [42, 43].

2.2. Numerical tools

The CFD model presented in Figure 1 was generated from the real engine geometry and simulated using the CONVERGE CFD software [44], a commercial code based on the Finite Volume method and developed particularly for ICE applications. A detailed sketch of pre-chamber is shown in the same figure. As it can be seen, it is installed at the cylinder head with a small inclination respect to the cylinder axis. This offset is attributed to the particular design of the cylinder head, which did not allow for a symmetrical installation of the pre-chamber. The bottom right corner of the figure shows the layout of the pre-chamber holes. Due to these constraints, the nozzles orientation was optimized to guarantee the maximum free path for the hot jets.

A summary of the model setup is presented in Table 3, with the most relevant physical models, numerical schemes and details of the mesh. A broader description of the CFD model and a more detailed explanation of the chosen configuration parameters is described in previous researches [45, 41].

Boundary and initial conditions for the simulations were configured based on the available experimental data. The instantaneous pressure signal measured in the intake and exhaust ports was used as boundary condition for the inflow and outflow of the computational domain. Moreover, the wall temperatures of the domain were estimated from the lumped model proposed by Torregrosa et al. [46]. Regarding the mixture formation process, a perfect premixed mixture of gasoline/hydrogen and air was considered at the intake boundary condition (no spray modeling was performed). Besides, the stratification of residual gases remained inside the pre-chamber and the cylinder was considered in the simulations by initializing both regions with the combustion products of the previous cycle.

Table 2: *Experimental baseline test conditions.*

PC ignition baseline	
Engine speed [rpm]	4500
IMEP [bar]	12.8
Injected fuel [mg/cc]	28.4
Intake air temperature [K]	283
Intake pressure [bar]	1.1
Exhaust pressure [bar]	1.07
coolant and oil temperature [K]	363

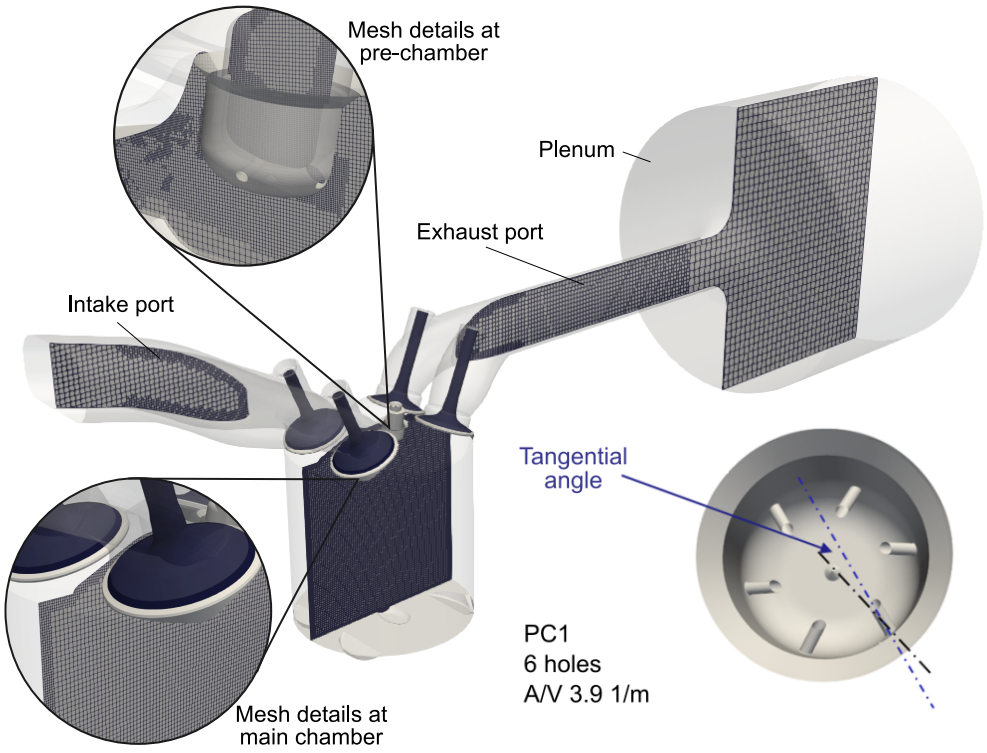

Figure 1: *Computational domain and mesh details. The pre-chamber characteristics and layout of the holes is shown in the bottom right corner.*

The ECFM combustion model is well suited for describing the propagation of turbulent premixed flames [47, 48]. However, it does not solve detailed chemistry. Thus, the auto-ignition delay and laminar flame speed values of the mixture need to be accounted for by data tables. In a previous work by the authors [45], these tables were generated by a set of 0D well-stirred reactor calculations for the auto-ignition delay times and 1D simulations for the laminar flame speed in a wide range of temperature, pressure, equivalence ratio and composition of the mixture. An example of these calculations is shown in Figure 2 where the results for different reaction mechanisms [49, 50, 51, 52, 53] are plotted and compared with experimental data [54, 55]. Finally, as the mechanism from Liu et al. [49] gave the most accurate predictions at engine-like conditions, it was selected to generate the data tables.

As an additional step for increasing the reliance of the model, the selected mechanism was also validated considering both gasoline/H_2 and pure hydrogen combustion. Results of this procedure are presented in Fig. 3, where an example of validation is shown using the experiments performed by Mandilas et al. [56] and, Ravi and Petersen [57]. In both cases, the model reasonably captures experimental trends when modifying the air-to-fuel ratio. Indeed, simulations offer a good estimation of the laminar flame speed considering a 5% of H_2 fuel blend at high λ values. These outcomes exhibit the accuracy of the model for predicting combustion fundamentals of gasoline/hydrogen fuel blends, providing a good starting point to establish reliable conclusions related to engine operation.

Nevertheless, due to the lack of experiments available in the literature for gasoline/hydrogen blends considering realistic engine conditions, results of this methodology must be further validated considering real engine experiments to corroborate the observed trends.

In this investigation, the adjusted tables of laminar flame speed and auto-ignition delay were calculated considering several amounts of hydrogen enrichment in the gasoline fuel blend. This will be further explained in the next section.

2.3. CFD model validation

In previous studies [45, 41], the authors have explained that the ECFM combustion model has some limitations when performing simulations with high λ values. Mainly, simulating the flame propagation through the pre-chamber nozzles, which is more critical as the nozzle diameter is reduced or the air-dilution level is increased, is very challenging, specially the aspects related to the flame quenching.

Literature suggests that the ECFM model uses a flame speed correction factor when the flame approaches the walls, reducing the laminar flame speed and thus taking into account the flame extinction [58]. However, accurately modelling all the physical phenomena involved in this process is still very complicated. Furthermore, a calibration of the CFD model is required to ensure that the results are reproducing well enough the global engine performance while ensuring a

Table 3: *CFD model configuration.*

Physical models	
Turbulence	URANS RNG k-ϵ
Combustion	ECFM
Equation of state	Redlich-Kwong
Ignition	imposed stretch spark ignition model (ISSIM)
Numerical schemes	
Spatial discretization	Second-order central difference scheme
Temporal discretization	First-order central difference scheme
Coupling between transport equations	PISO algorithm
Mesh details	
Cell size in the cylinder	1 mm
Cell size in the pre-chamber	0.25 mm scheme
Cell size in the pre-chamber walls & holes	0.125 mm
Minimum cell size by AMR	0.125 mm

proper study of the underlying physical phenomena. Therefore, considering the operating point described in Table 2, the in-cylinder pressure and HRR from the simulations were compared to those measured in the single cylinder engine at stoichiometric conditions and at the air-dilution limit (λ = 1.6).

The calibration results are shown in Figure 4, where the average in-cylinder pressure signal of the 250 measured engine cycles is plotted along with the corresponding HRR pro-

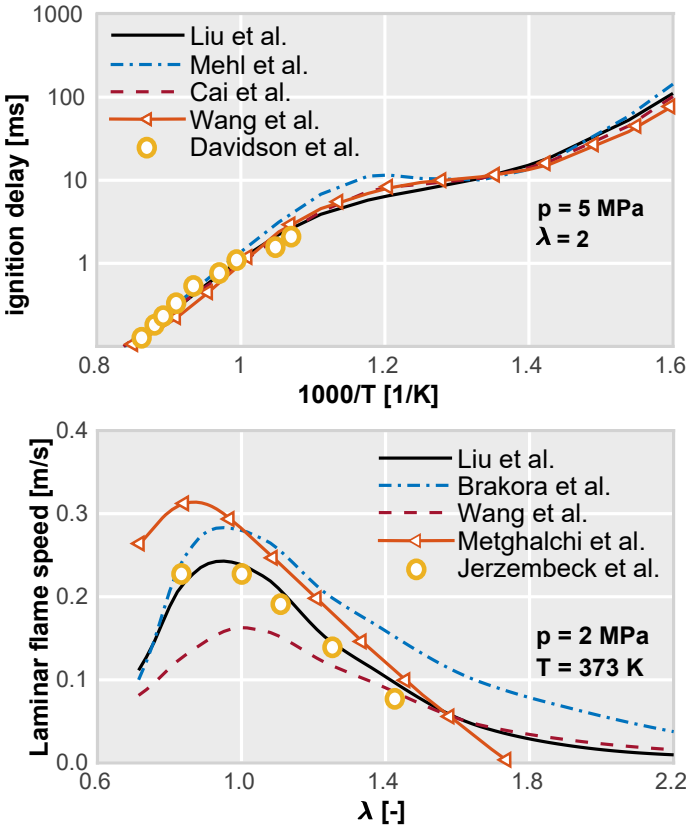

Figure 2: *Auto-ignition delay and laminar flame speed validation for different gasoline surrogates mechanisms at engine-like conditions.*

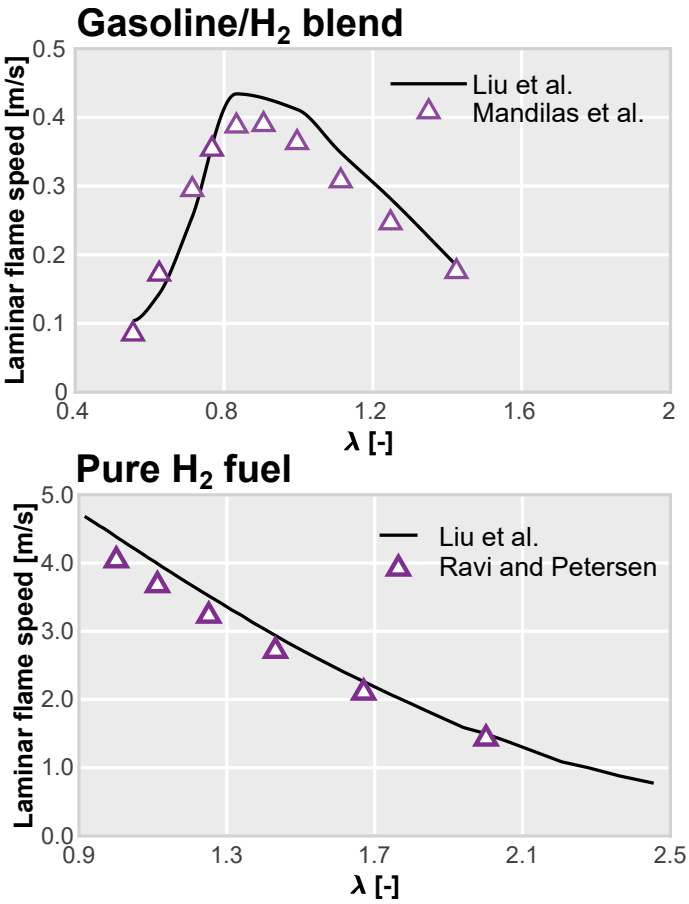

Figure 3: *Laminar flame speed validation for H_2 combustion. Results of a gasoline/hydrogen blend (5% of H_2) at 5 atm and 360K using the experiments of Mandilas et al. [56] (top). Results of pure hydrogen combustion at 1 atm and 443K using the experimental data of Ravi and Petersen [57] (bottom).*

file (estimated from the combustion diagnosis tool) for both λ values. A good agreement can be observed between the simulated and experimental pressure data, since simulated signals are within the experimental uncertainty due to the cycle-to-cycle dispersion. In this figure, the uncertainty due

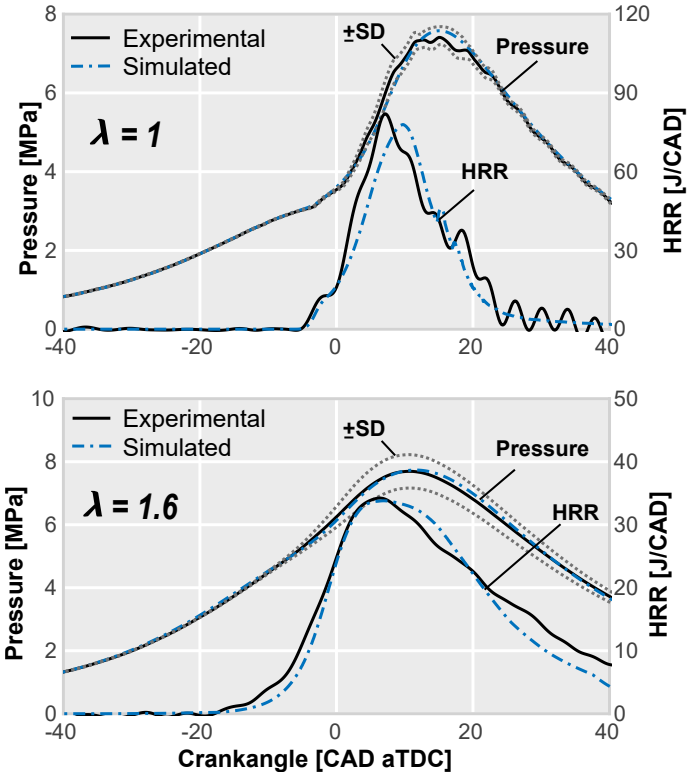

Figure 4: *Experimental validation of the CFD model in terms of in-cylinder pressure and rate of heat release operating at stoichiometric (top) and diluted conditions (bottom).*

to this cycle variability is assessed by the point-to-point Standard Deviation (SD). Additionally, the numerical model is also able to capture properly the HRR trace, showing a good ignition onset and both maximum combustion rate and duration.

2.4. Methodology

The first stage of this research work consisted in performing an experimental campaign of the engine at high load and high speed conditions (shown in Table 2) with the purpose of highlighting the benefits of the pre-chamber ignition concept against conventional spark-ignition. The measurement methodology followed in this campaign was the same as previous works from the authors [36, 59]. This methodology consisted in adjusting the injected fuel mass to obtain the target gross Mean Effective Pressure (IMEP) operating with the conventional SI system, and keeping it constant for the subsequent pre-chamber tests. A Spark Timing (ST) sweep was performed in each experiment until the Maximum Brake Torque (MBT) was reached, or by contrast, until a continued ST advance was prevented by knocking combustion.

Next, a λ sweep was performed for both ignition systems. The air-dilution level was increased until the cycle-to-cycle variability prevented a suitable engine operation due to excessive misfires. The fuel mass was maintained (same as the stoichiometric test) and the intake pressure was increased until the desired mixture composition was achieved (degree of air-dilution).

Following the experimental activities, the CFD model was set up and calibrated to the reproduce the experimental trends, as shown in Figure 4. However, the dilution limit of $\lambda = 1.6$ achieved with the passive pre-chamber was still not sufficient to reduce the levels of NO_x emissions below the European standards without the use of the TWC. For this reason, the second stage of this paper consisted in a numerical evaluation of the pre-chamber ignition system with the use of hydrogen, completely mixed with the gasoline fuel at the intake port, in order to extend the dilution limit measured in the experiments.

In this case, a dilution level of $\lambda = 1.9$ was selected and several CFD simulations were configured in this new operating condition. As the previous simulations were set up with the same parameters as their respective experiments (boundary and initial conditions, spark timing, etc), the simulations at $\lambda = 1.9$ were configured following the same methodology. Therefore, the fuel mass was adjusted to release the same amount of energy as the previous simulations and the intake pressure was increased to achieve the target air-to-fuel ratio (almost twice the pressure of the stoichiometric case). Moreover, as it was not possible to operate the engine in this point, the other boundary and initial conditions were taken from the dilution limit experiment.

A previous 0D and 1D study was performed using the utilities described earlier in this section for generating the laminar flame speed and auto-ignition delay data tables for the CFD combustion model. With this study the amount of hydrogen required to recover competitive burning rates at these highly diluted conditions was estimated. Then, the passive pre-chamber ignition concept using gasoline/hydrogen blends injected in the intake port was numerically evaluated. Combustion features were extensively analyzed and compared for all simulations in order to make a proper evaluation of the H_2 addition strategy.

3. Results and discussion

This section discusses the main findings of this work, starting form the experimental campaign to establish the dilution limits of both SI an TJI concepts, and moving on towards the numerical assessment of implementing hydrogen to enhance combustion.

3.1. Determination of the dilution limits

Results from the reference stoichiometric test are shown in Figure 5 where the measured in-cylinder pressure and the estimated HRR profiles are plotted for both ignition systems. The shaded areas correspond to the point-to-point standard deviation of all measured cycles, which give an estimation of the cycle-to-cycle variability (CCV) of each test. These curves clearly evidences the benefits of the pre-chamber ignition system over conventional spark-ignition [36, 59, 41]. The increased burning velocities shown in the bottom plot causes

an increment in the maximum pressure peak (over 50%) and also allow to shift the combustion phasing (CA50) towards TDC.

A quantitative comparison of the most relevant combustion parameters is presented in Figure 6. The graphs show an efficiency gain around 3% when switching from SI to TJI. This benefit is mainly due to the improved combustion phasing (14 CAD closer to TDC) achieved by reducing the combustion duration.

The Maximum Amplitude Pressure Oscillation (MAPO) is also plotted to give an indicator of the knocking intensity. A maximum tolerance of 1.5 bar was considered above which the engine integrity was compromised. Due to the extreme sensitivity of the knocking trend when advancing the spark timing, it was not possible to set a combustion phasing that gives comparable TJI values of MAPO. Note that in this situation, a small change on this parameter (±0.5 CAD) meant switching from a safe situation (MAPO values well below 1.5 bar) to critical conditions (MAPO > 10 bar). Therefore, the combustion phasing of the SI test could not be completely optimized as the engine was limited by extreme knock after a certain ST was exceeded. Nevertheless, it is clear that even considering this slight spark timing advance (0.5 CAD), the combustion phasing should be far from the TJI test. The last graph shows the improvement of the CCV though the IMEP variability parameter (σIMEP). It is noticeable that the PC ignition system significantly reduces the cyclic dispersion. This

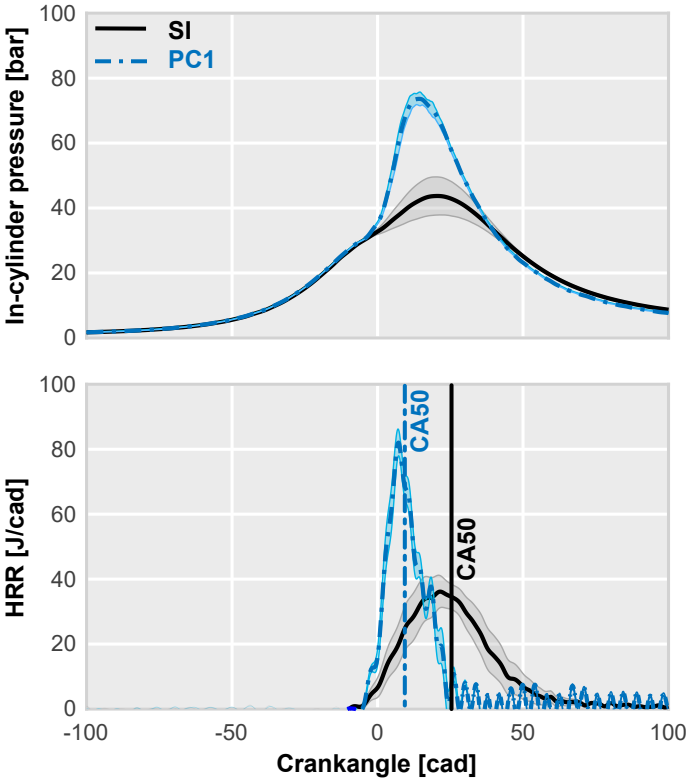

Figure 5: *Experimental in-cylinder pressure and HRR traces for the SI and passive TJI systems at stoichiometric conditions.*

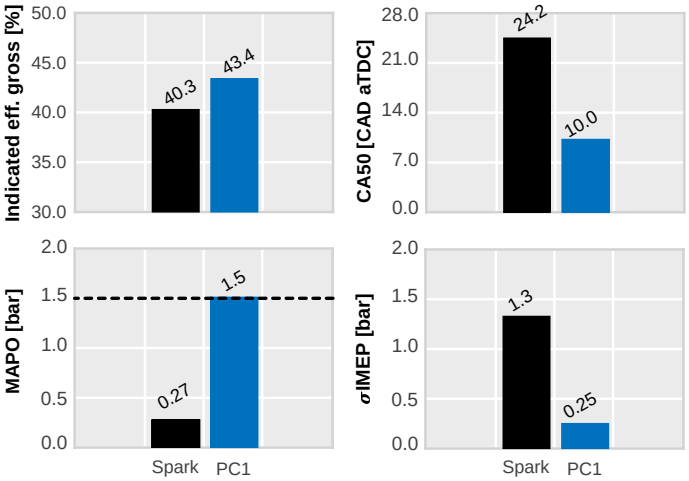

Figure 6: *Comparison of combustion-related parameters between SI and passive TJI concepts at stoichiometric conditions.*

is evidenced by a decrease of almost 80% in the σIMEP value with respect to the conventional SI value. The combination of all these benefits result in a considerable improvement of the engine performance, particularly at those operating conditions were the enhanced burning rates allow to push combustion towards TDC where the conventional SI system is limited by knocking combustion.

After the stoichiometric test, a λ sweep was performed following the measurement methodology described in previous sections and results are presented in Figure 7. In this case, indicated efficiency trends observed at stoichiometric conditions are mostly kept throughout the whole dilution range. This parameter is always higher with TJI and CCV is reduced (except for the $\lambda = 1.2$ case). The maximum dilution limit reached with the passive pre-chamber ($\lambda = 1.6$) is 20% higher than the limit of the conventional SI system ($\lambda = 1.4$).

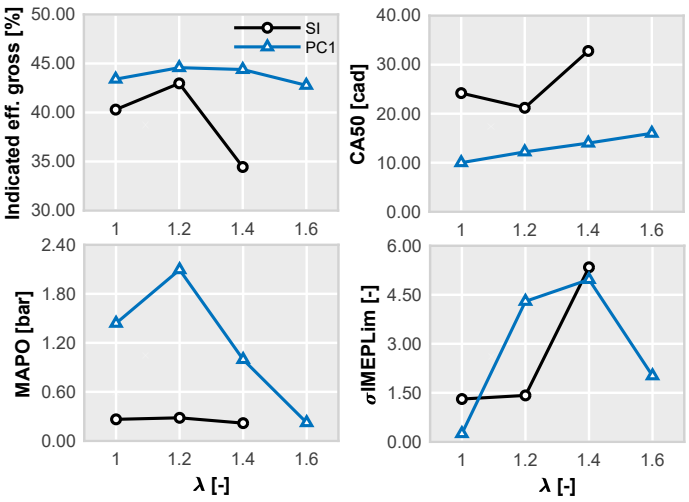

Figure 7: *Trends of the most relevant engine outputs at different levels of air-dilution.*

Although the engine efficiency is kept at considerably high values when operating at the maximum dilution limit, this level of dilution is not sufficient to fulfill current pollutant regulations without the use of a TWC. This represents a major issue, given that the TWC is not able to operate without a stoichiometric mixture composition in the exhaust tailpipe. Nonetheless, considering that the passive pre-chamber concept was able to inherently increase the maximum air-dilution range admitted by the engine, it is interesting to evaluate potential paths to enable the operation of this concept under leaner conditions, in order to reduce the levels of NO_x after combustion to near zero values, while maintaining, or even improving, the engine thermal efficiency.

In this case, as the flame propagation in the main chamber is extremely compromised, the use of hydrogen to further enhance combustion characteristics arises as a promising solution to achieve this target. Thus, in the following studies an optimum dilution level was determined by 1D laminar flame speed calculations considering a suitable amount of H_2 addition. Thereafter, an operating condition characterized by the determined air-to-fuel ratio and hydrogen volume fraction was set up and numerically simulated to study its impact on combustion and engine efficiency.

3.2. Preliminary studies using hydrogen fuel

A preliminary evaluation of the hydrogen fuel was performed to give an idea about the required H_2 amount. The 0D and 1D utilities used to generate the reference data tables for laminar flame speed and auto-ignition delay times were used here to determine a suitable range for the hydrogen addition, and subsequently generating the new data tables considering the appropriate gasoline/hydrogen blends.

The percentages of hydrogen presented in this research work are considered in volume fractions with respect to the total air admitted during the intake stroke. The results of the 1D laminar flame speed simulations are shown in the colour maps of Figure 8. A λ sweep was performed extending from stoichiometric to $\lambda = 2$ conditions, and the amount of hydrogen was also swept from 0 until 20% of the total air volume. The λ values shown in the map were simulated considering representative values of the in-cylinder pressure at the spark timing and a constant temperature of 800K. Both parameters were estimated by thermodynamic calculations based on engine tests and simulations [36]. In addition, the total energy available in all fuel mixtures (gasoline+hydrogen) is also constant.

The top plot of Figure 8 shows a pathway towards recovering the laminar flame speed of the $\lambda = 1.6$ no H_2 case (experimental air-dilution limit). A λ value of 1.9 was considered to be a suitable dilution level for performing the CFD simulations. Additionally, the bottom plot shows that including hydrogen also reduces the flame thickness, which is considerably enlarged when moving from $\lambda = 1$ to $\lambda = 1.9$ conditions. This has some relevant implications regarding the flame structure, and thus, the regime in which combustion progresses [60].

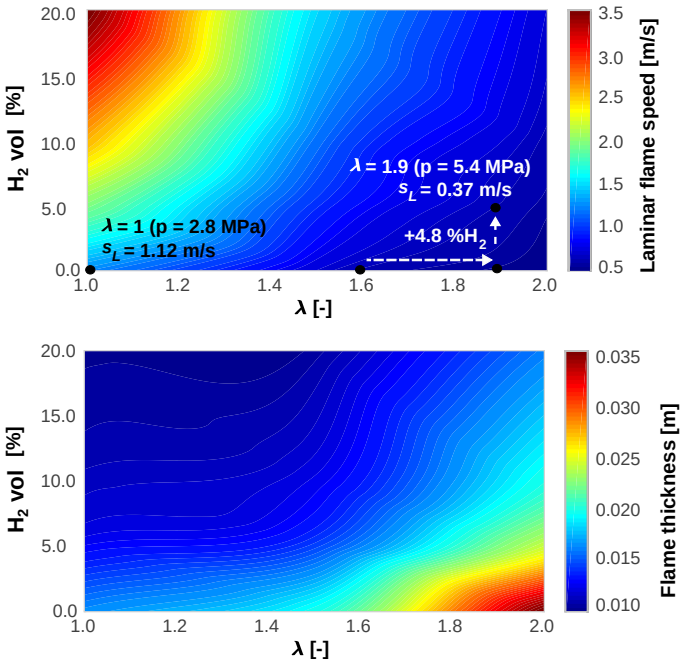

Figure 8: *Laminar flame speed and flame thickness for different levels of air-dilution and different percentages of hydrogen.*

Moreover, the auto-ignition delay calculations were also performed for the same λ and hydrogen amount sweeps. From previous investigations [61], it is known that the trends of the ignition delay pivot around a certain temperature value ($\sim$ 950K) when enriching the gasoline fuel with hydrogen. Thus, the impact of this enrichment could change drastically when considering values above or below this threshold.

The unburned gases temperature were computed from the experimental tests at stoichiometric and maximum dilution conditions to select an appropriate temperature for the 0D calculations. They were included in the top plot of Figure 9 for reference. A temperature value of 900K was chosen for reference as it is well representative of the unburned temperature ranges reached by the gases when combustion is progressing in the main chamber.

Results are shown in the colour map plotted at the bottom graph of Figure 9. As expected from the literature, the ignition delay values tend to decrease when considering higher dilution rates due to the increased pressure achieved within the combustion chamber. However, the addition of hydrogen tends to increase the auto-ignition delay, reducing thus the knocking appearance.

This study highlighted the benefits of hydrogen for enabling a successful lean operation of the engine. Therefore, the data tables of laminar flame speed and auto-ignition delay were generated considering the established hydrogen ranges and a subsequent evaluation of the pre-chamber ignition concept enhanced with this alternative was performed with the CFD model.

3.3. Modelling the passive pre-chamber ignition concept fuelled by gasoline-hydrogen blends

Once the preliminary study of the fuel was concluded and the data tables generated, three engine simulations were calculated at $\lambda = 1.9$ conditions in order to evaluate different levels of hydrogen (2.5%, 4% and 5%) and their impact on the pre-chamber and main chamber combustion. These simulations were configured by considering the same methodology used in the experimental campaign. For this purpose, the mass of gasoline was adjusted in order to release the same amount of energy as the stoichiometric test, considering the specific amount of hydrogen added in each case. Thus, as the percentage of hydrogen increased, the mass of gasoline further decreased whereas the intake pressure was also increased to achieve the target air-to-fuel ratio. As no experimental data was available for these conditions, the spark timing used in each case was kept equal to the $\lambda = 1.6$ simulation, given that the preliminary studies showed that the burning velocities should be similar to this case.

3.3.1. Analysis of the pre-chamber combustion

This section focuses on analysing the first stage of the combustion process, that is the pre-chamber burning process and the ejection of hot gas characteristics.

Results of the pre-chamber combustion characteristics are shown in Figure 10. Due to the loss of laminar flame speed, a considerable worsening of the HRR profile is observed when moving from stoichiometric to $\lambda = 1.6$ conditions, both reducing the maximum burning rate and increasing the combustion duration. However, with the hydrogen inclusion, the HRR profile no longer worsens when further increasing the air-dilution up to $\lambda = 1.9$. As expected from the preliminary studies, the combustion profiles of the three levels of H_2 are very similar to the $\lambda = 1.6$ case, achieving a slight improvement of 2 CAD in the combustion duration when considering 5% of hydrogen, as shown in Table 4.

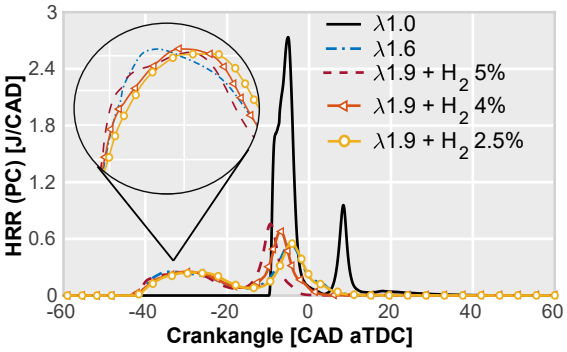

Figure 10: *Pre-chamber combustion characteristics for different levels of hydrogen enrichment.*

A visualization of the pre-chamber combustion is depicted in Figure 11, where a comparison between the reference $\lambda = 1$ and $\lambda = 1.6$ cases is made, including the most favorable H_2 simulation (5%). An axial cut plane parallel to the pre-chamber axis was used for each snapshot representation. The source term of the energy equation is coloured to track the flame front. Each snapshot is referenced to a crank-angle degree after the spark timing (CAD aST).

The premixed flame is clearly observed in the three cases, that is a well established flame front which sweeps the whole pre-chamber volume. However, the most relevant difference between the snapshots is the time frame. For both $\lambda = 1.6$ and $\lambda = 1.9$ cases, the flame takes longer to reach the orifices intake, almost four times more than the stoichiometric simulation. The pre-chamber pressurization is a key aspect for obtaining high quality reacting jets [36]. With the purpose of analysing this aspect, the pre-chamber relative pressure (Δp), defined as the pressure difference between the pre-chamber and the main chamber, is included in the bottom plot of Figure 11. As it can be seen, all diluted cases do not achieve a suitable pressurization due to the very slow combustion process.

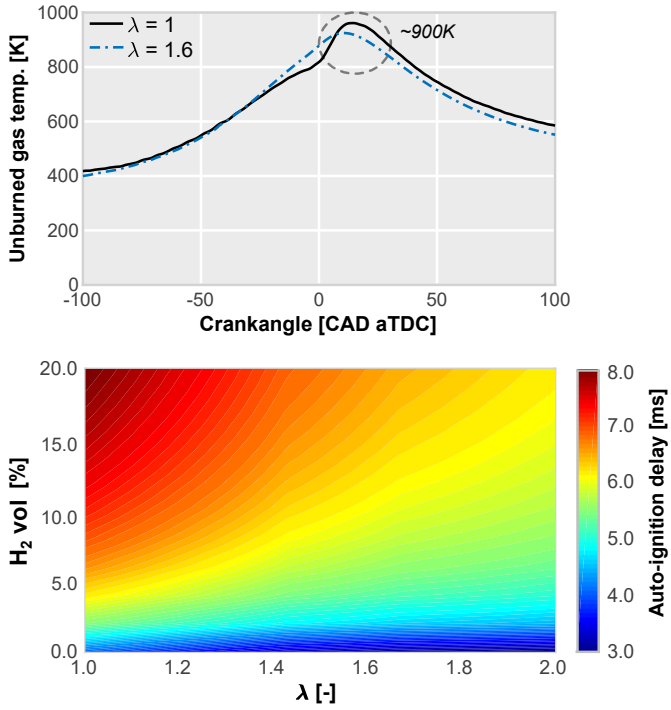

Figure 9: *Auto-ignition delay values for different levels of air-dilution and different percentages of hydrogen considering an unburned gas temperature of 900K.*

Table 4: *Pre-chamber burn durations.*

Case	Combustion duration [CAD]
$\lambda = 1.6$	22.8
$\lambda = 1.9 + 2.5\%\ H_2$	24.4
$\lambda = 1.9 + 4.0\%\ H_2$	22.7
$\lambda = 1.9 + 5.0\%\ H_2$	20.7

The former remark is confirmed when analysing the penetrations (referenced to the moment of ejection) plotted in Figure 12, which correspond to the jet with the longest gap to travel within the combustion chamber. The faster combustion of the stoichiometric simulation results in considerably better jet features than for the lean cases, achieving much higher penetration rates in the first stages of the ejection process and reaching a higher maximum value in less time.

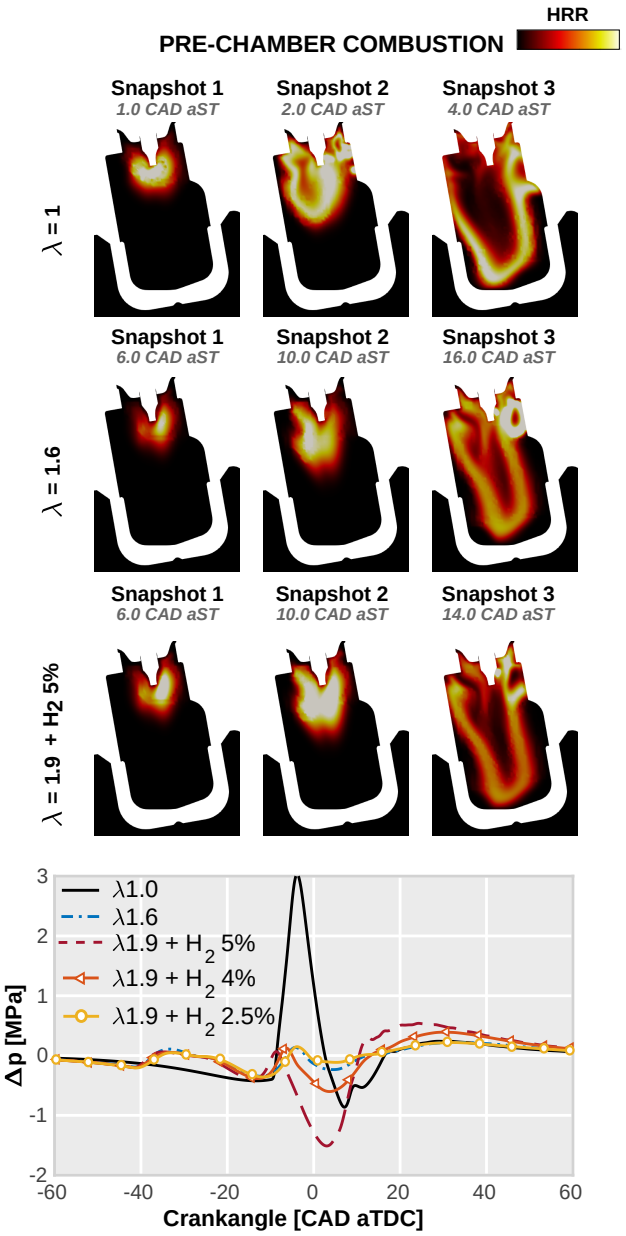

Figure 11: *Pre-chamber ignition sequence for the $\lambda = 1$, $\lambda = 1.6$ and $\lambda = 1.9 + 5\%$ H_2 cases. The source term of the energy equation is coloured to track the flame front at a given snapshot. The HRR of each case is divided by the corresponding maximum value for visualization purposes. The pre-chamber relative pressure (Δp) is shown in the bottom plot.*

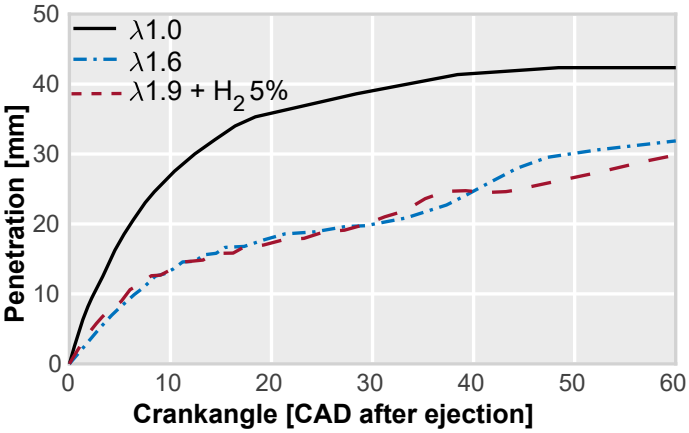

Figure 12: *Jet penetration rate of the $\lambda = 1$, $\lambda = 1.6$ and $\lambda = 1.9 + 5\%$ H_2 cases. The jet with a longer gap to travel within the combustion chamber is only included for simplicity.*

However, the combustion profiles of the lean simulations are not only attributed to the lower laminar flame speeds, but also to the spark timing. As proven in [41], the advance in spark timing, necessary to achieve an optimum combustion phasing when using external dilution strategies, has detrimental consequences for the pre-chamber combustion process. Due to the inherent worsening of the flow field conditions (residual gases, velocity and turbulence fields) the combustion stability is notably compromised.

In order to highlight this remark, non-reacting simulations (motoring conditions) of the $\lambda = 1$ and $\lambda = 1.9 + 5\%$ H_2 cases were carried out at 4500 rpm. The velocity and turbulent kinetic energy (TKE) fields in the pre-chamber were plotted at -10 CAD and included in Figure 13. Although the addition of hydrogen does not suppose a relevant impact on the internal aerodynamics of the cylinder, the pressure increase required to achieve a dilution level of $\lambda = 1.9$ can condition the flow inside the pre-chamber. It can be observed that the magnitude of both fields increases at lean conditions, especially in the bottom part of the pre-chamber, close to the holes inlet. Thus, the spark timing should be optimized when implementing the H_2 dilution strategy to further enhance the performance of the engine.

3.3.2. *Analysis of the main chamber combustion*

The second stage of combustion is analysed in this section. Here, the main chamber combustion and the root causes of burning rate variations when adding hydrogen are discussed.

Moving on towards the analysis of the main chamber combustion features, the results in terms of in-cylinder pressure and HRR profiles are shown in Figure 14. Despite the initial assessment from the 1D flame speed calculations, adding 5% of hydrogen allows to achieve a similar combustion profile to the $\lambda = 1$ case. Thereafter, as the percentage of included hydrogen decreases, the combustion tends to deteriorate. However, even the smallest amount of H_2 considered in this study is able to burn at $\lambda = 1.9$ similarly to the experimental dilu-

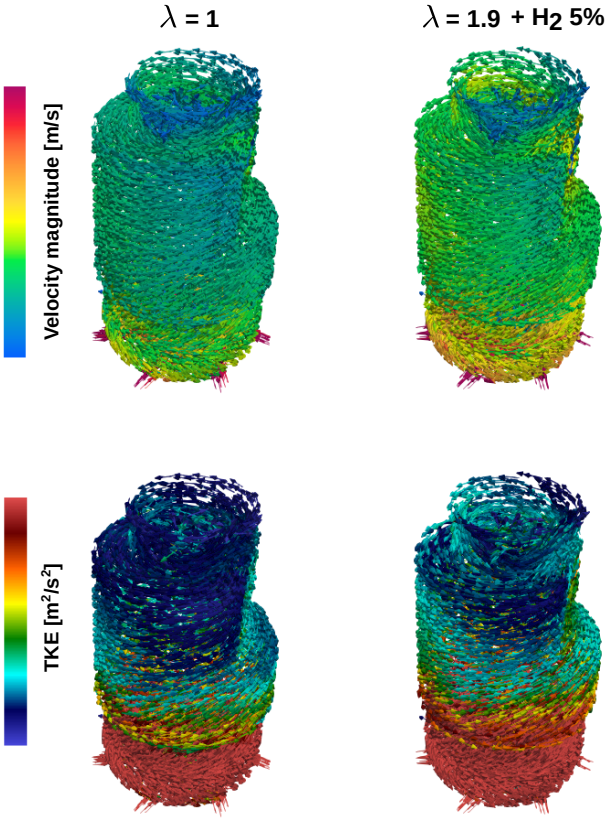

Figure 13: *Velocity and TKE fields inside the pre-chamber at -10 CAD for the $\lambda = 1$ and $\lambda = 1.9 + 5\%\ H_2$ cases.*

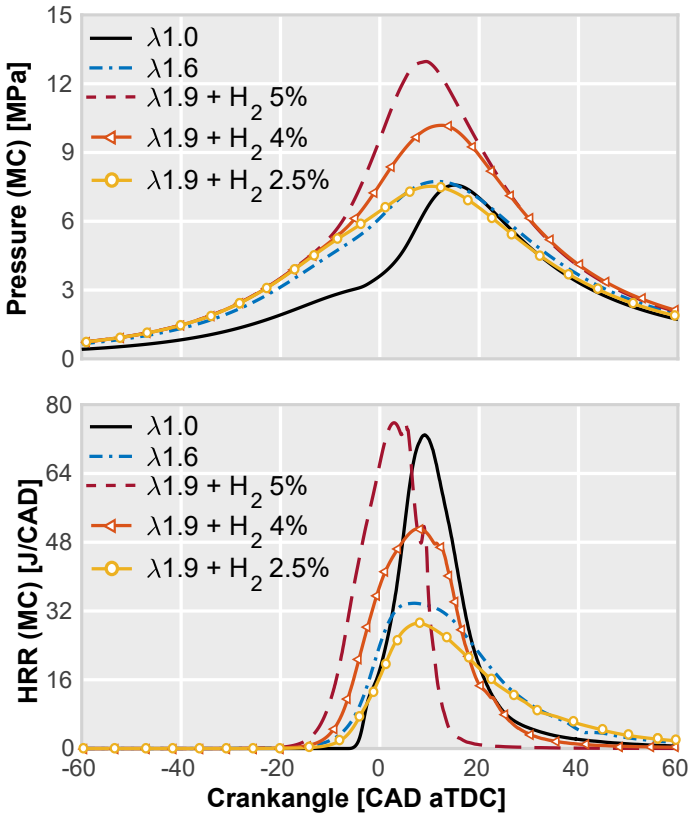

Figure 14: *Main chamber combustion features of different levels of hydrogen enrichment. The simulated pressure profile and HRR trace in the main chamber are included.*

tion limit in the main chamber. Thus, it is feasible that just by adding 2.5% of hydrogen in the intake port could extend the dilution limit up to $\lambda \sim 1.9$.

Figure 15 shows the root causes of the observed combustion enhancement. In the top plot, the laminar flame speed is depicted. Here, the time scale is referred to the spark timing of each case. In the first stage, during the pre-chamber combustion, a large gap in the laminar flame speed is observed among the lean and the stoichiometric cases. However, as expected from the 1D studies presented in Figure 8, the difference between the laminar flame speed of the diluted ($\lambda = 1.6$) and H_2-enriched cases (with 2.5%, 4% and 5%, respectively) is practically negligible when the flow temperature is kept constant. This is confirmed by inspecting the bottom plot of Figure 15, where the unburned gas temperature is plotted and no remarkable differences are observed for the lean cases during the first stage of combustion. On the contrary, the laminar flame speed significantly increases after the onset of combustion in the main chamber and the gap among the diluted cases becomes wider. This is attributed to the increase of the unburned gas temperature, also shown in the bottom plot of Figure 15. In this combustion stage, the temperature of fresh gas reaches higher values as combustion progresses when the amount of hydrogen is progressively incremented. This effect causes an increment in the combustion rate that, in some cases, can even exceed the values of the stoichiometric case.

A detailed visualization of the main chamber combustion process is shown in Figure 18 in order to analyse the characteristics of the flame propagation in this region. The $\lambda = 1$, $\lambda = 1.6$ and $\lambda = 1.9 + 5\%\ H_2$ cases were considered. The snapshots were drawn for a horizontal cut plane perpendicular to the cylinder axis and 3 mm away from the pre-chamber bottom. As with Figure 11, the heat release was coloured by the source term of the energy equation to track the flame front. The jet boundaries are highlighted as a green contour line, drawn with the help of a pre-defined dynamic tracer implemented in the code.

It is clearly observed in the ignition sequence of the stoichiometric case how the flame is initially sustained by the jets, which helps to boost the early phases of flame propagation. For the lean cases however, the poor jets play a small roll in the first stages of ignition, and the onset of combustion in the main chamber occurs later. In all cases the flame is able to progress outside the boundaries of the jets, nevertheless it is noticeable that for the hydrogen enriched case the flame leaves the jets before due to the enhanced thermo-chemical properties of the mixture.

This last remark can be also observed in the plots on the right side of Figure 18 which shows the energy release profile in the main chamber, considering the amount of energy released inside and outside the jets boundary. Both $\lambda = 1$ and $\lambda = 1.9 + 5\%$ H_2 cases follow the same trend, releasing a minor part of the total energy (less than 20%) inside the jets. However, the energy released inside the jets for the hydrogen-enriched case is almost half of the corresponding energy in the stoichiometric case. On the contrary, the percentage of energy released inside the jets for the $\lambda = 1.6$ case is higher than for the other two cases. This is mainly due to the poor thermo-chemical conditions of the mixture, which impedes the flame front from quickly surpassing the jets boundary, forcing combustion to be established within these limits where the conditions of turbulence are more favourable.

Another interesting remark comes from results included in Figure 16, where the spatially-averaged values of turbulent kinetic energy in the main chamber are plotted for the aforementioned non-reacting simulations of the $\lambda = 1$ and $\lambda = 1.9 + 5\%$ H_2 cases. Small differences are observed between both curves, since the internal aerodynamics of the cylinder depend mostly on the intake port design and the engine speed and both remain unchanged in the investigation. However, the gap between the onset of combustion in the main chamber for both cases shows that the main chamber TKE levels are higher for the lean case. Thus, when enriching the mixture with 5% of hydrogen, not only the thermo-chemical properties favour the combustion process, but also the higher TKE levels at the onset of the main chamber combustion contributes to increase the burning rate.

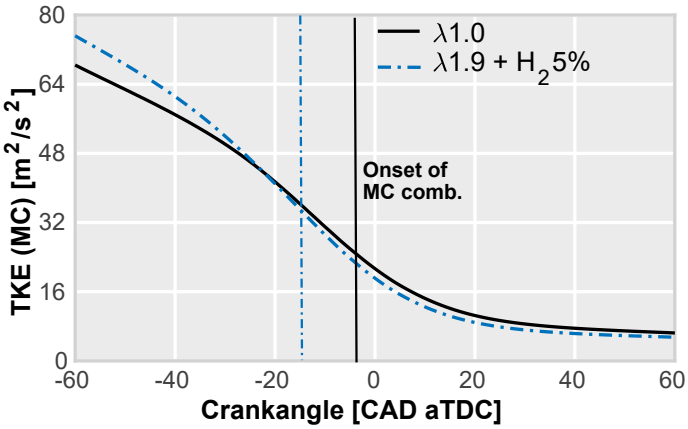

Figure 16: Main chamber TKE profiles for the non-reacting simulations at the studied operating condition.

3.3.3. Analysis of the flame regime

In this section, the evolution of the flame regime throughout the whole combustion process (from the pre-chamber to the main chamber) is analyzed to characterize the flame structure and how it affects the flame propagation.

In Figure 17 a Borghi-Peters diagram [60, 48] is included for analysing the turbulence-combustion interaction in the three cases considered so far. This diagram, also known as *flame regime diagram*, is used to analyse the structure of the flame as combustion progresses. Its computation is based on the laminar flame speed (S_L), flame thickness (l_f), turbulence length scale (l_t) and turbulent intensity (u'). The coloured dots represent the time frame respect to the spark timing during the combustion process.

The stoichiometric combustion progresses initially in the *thickened wrinkled flames* regime, where the Kolmogorov scales are larger than the flame thickness and the combustion rates

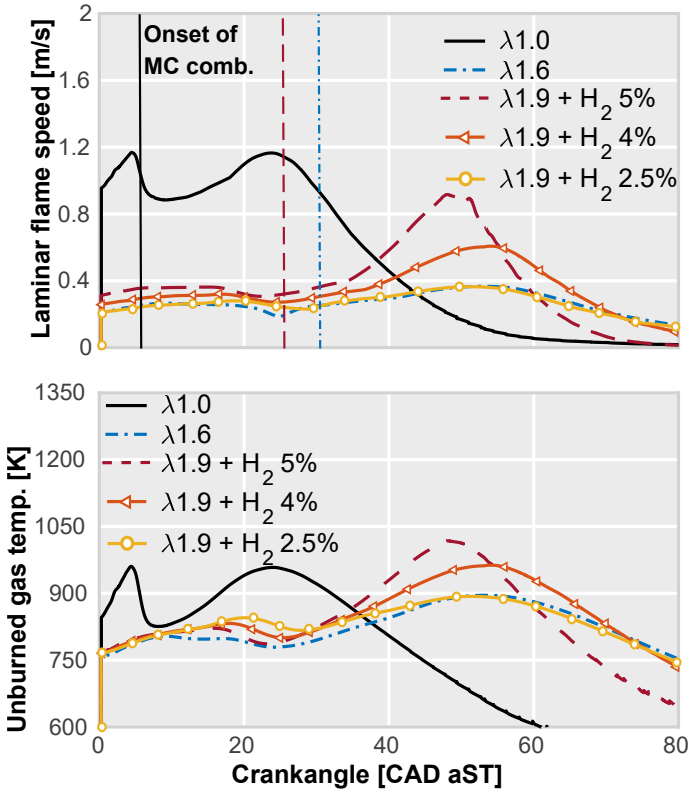

Figure 15: Laminar flame speed and unburned gas temperature for all simulations. The time scale is referenced to the spark timing of each simulation.

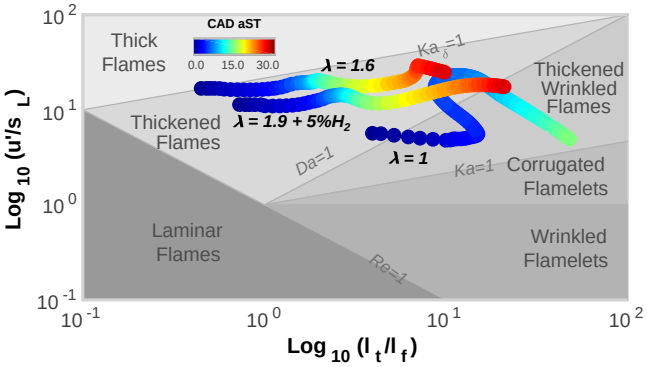

Figure 17: Flame structure as combustion progresses from the pre-chamber to the main chamber.

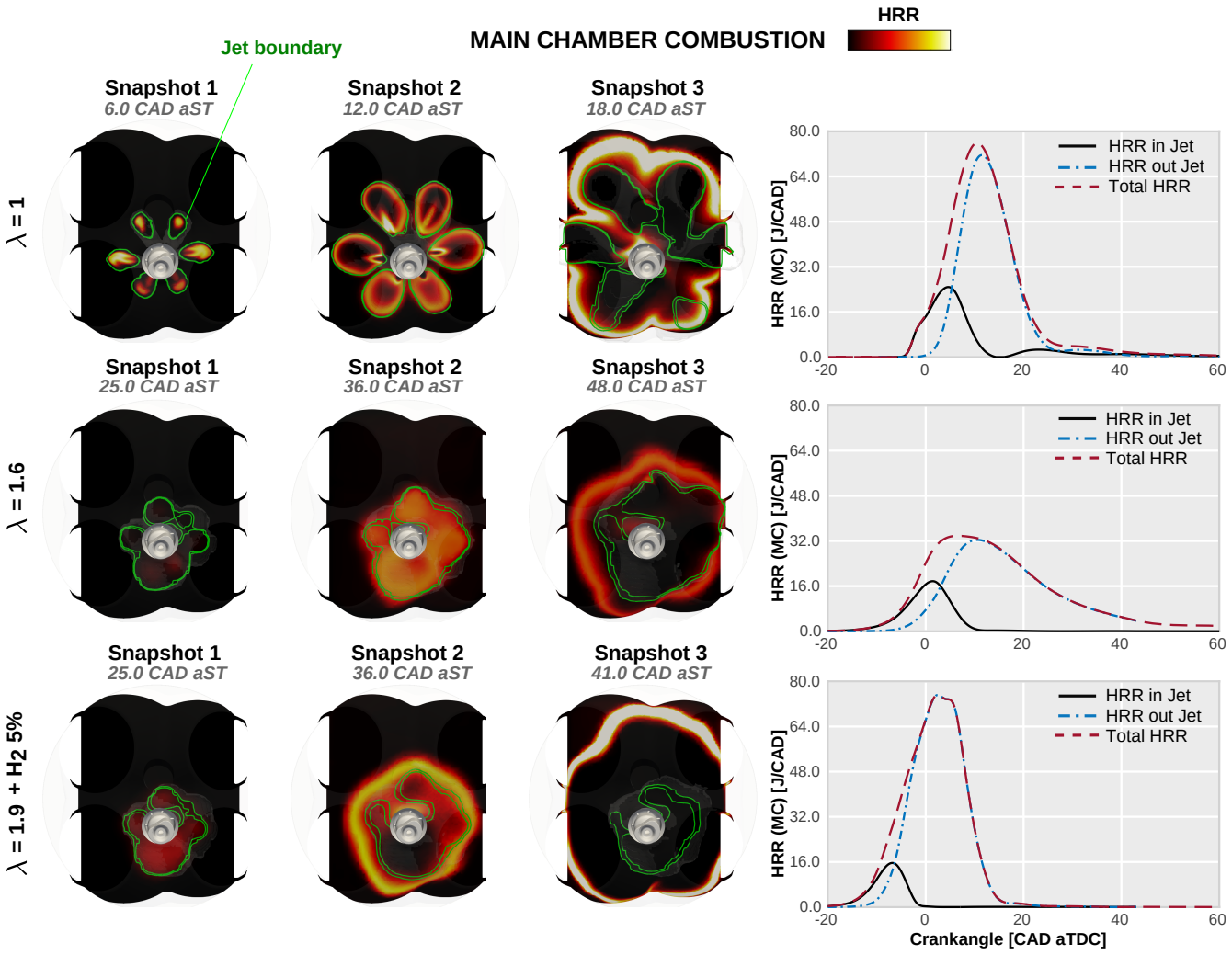

Figure 18: *Main chamber ignition visualization at $\lambda = 1$, $\lambda = 1.6$ and $\lambda = 1.9 + 5\%$ H_2 conditions. The source term of the energy equation is coloured to track the flame front at a given snapshot. The jet boundaries are highlighted in green and determined with a user-defined dynamic tracer. The numeric values and evolution of the HRR profiles inside/outside the jets for all simulations are also included.*

are suitable for most of the operating conditions studied for SI engines. Later on, due to the nature of the passive pre-chamber combustion concept, the flame shifts momentarily towards the *thickened flames* regime, where some eddies can penetrate into the diffusive layer of the flame structure. However, the flame quickly stabilizes and returns to the *thickened wrinkled flames* regime. On the other hand, the $\lambda = 1.6$ case begins in a less favourable region of the diagram, deeper into the *thickened flames* regime where the flame stability is compromised. Nonetheless, the hydrogen enriched case improves slightly the initial flame structure when compared to the $\lambda = 1.6$ case. Recalling Figure 8, this improvement is due to the combination of slightly higher laminar flame speed and lower flame thickness values achieved. At the end of the hydrogen-enriched curve, the flame structure shifts to a more favourable region. Thus, the properties of this fuel can inherently help to achieve a more stable combustion process even at extremely diluted conditions.

3.3.4. Impact on engine efficiency and pollutant emissions

Finally, this section discusses the impact of the enhanced burning rate due to the hydrogen-enriched blends over the engine thermal efficiency and NO_x formation.

Figure 19 shows the pressure-volume diagrams of the $\lambda = 1$ and $\lambda = 1.9 + 5\%$ H_2 simulations, from which an estimation of the indicated efficiency can be performed by a straightforward integration. As can be seen in Table 5, the pressure profile generated in the $\lambda = 1.9 + 5\%$ H_2 case increases the indicated efficiency by 3.7%, proving that, despite introducing the same amount of energy, the combination of the employed technological bricks (high air-dilution, passive pre-chamber ignition and H_2 addition) provides considerable benefits in terms of engine performance.

Additionally, the formation of NO_x within the cylinder is shown in Figure 20 for each simulated condition. The top plot depicts the temporal evolution of NO_x species during the

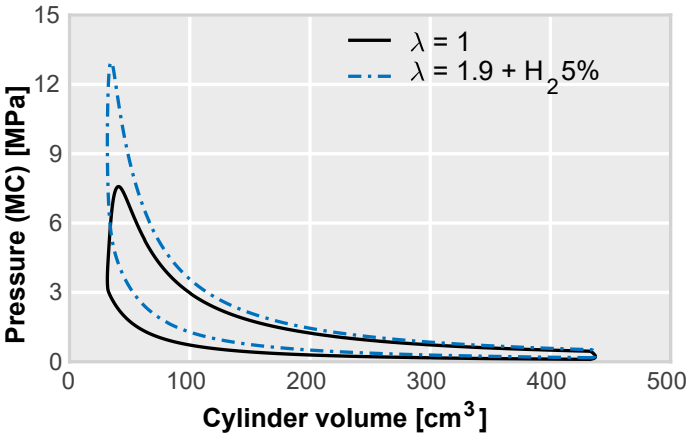

Figure 19: *P-V diagrams for the $\lambda = 1$ and $\lambda = 1.9 + 5\%$ H_2 cases. The pumping losses were not included to evaluate only the work produced in the firing cycle.*

Table 5: *Indicated efficiency for the simulations.*

Case	Ind. efficiency [%]
$\lambda = 1$	43.37
$\lambda = 1.6$	42.89
$\lambda = 1.9 + 5\%$ H_2	47.12
$\lambda = 1.9 + 4\%$ H_2	44.92
$\lambda = 1.9 + 2.5\%$ H_2	42.07

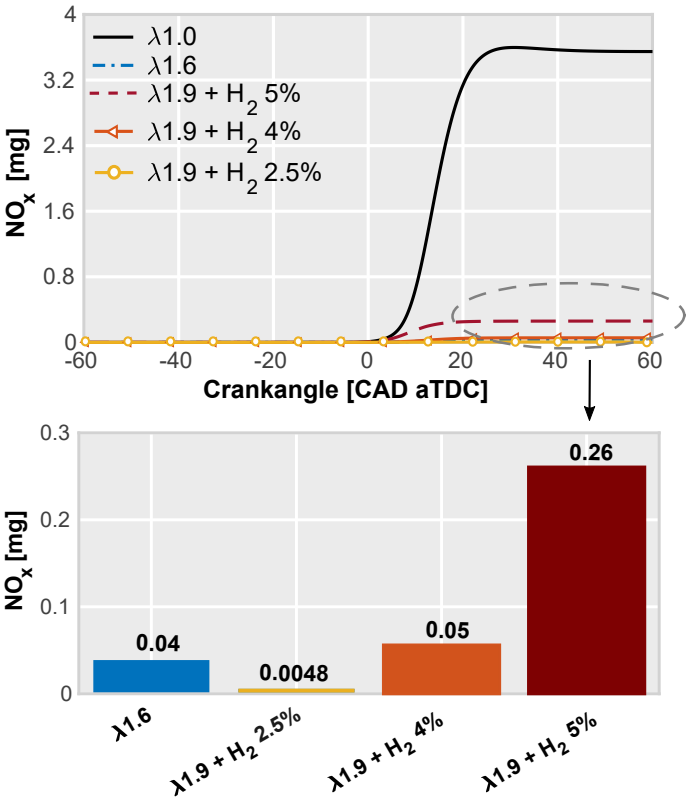

Figure 20: *NO_x formation in the cylinder for all the simulated cases. The bar graphs represent the NO_x value of each case at the end of the simulation.*

combustion cycle, while the bottom graph shows the NO_x amount at the end of the combustion cycle. As it can be seen, diluting the air-fuel mixture with air reduces the NO_x emission around 10 times if it is compared against the pure gasoline stoichiometric case. On the contrary, increasing the amount of hydrogen within the fuel blend increases the NO_x formation. This fact can be explained by the increment of flame temperature caused by the increase of the unburned gas temperature discussed above.

An interesting analysis can be made by comparing the NO_x emissions of the hydrogen-enriched cases with the values of the $\lambda = 1.6$ case. The NO_x formation increases significantly (about 7 times higher) by adding 5% of hydrogen. This value barely changes when considering 4% of H_2 enrichment, where the thermal efficiency is 1.6% higher than the gasoline stoichiometric case. Moreover, NO_x emissions are reduced by a factor of 10 when by considering 2.5% of H_2 enrichment. These results are encouraging as in this condition the efficiency levels of the engine are maintained within a suitable range (above 42%) while maintaining NO_x emissions below the required standards without the use of a three-way catalyst.

4. Summary and conclusions

A numerical methodology for evaluating the use of hydrogen combined with a passive pre-chamber ignition system in a turbocharged gasoline SI engine is presented in this paper. The numerical model, being successfully validated by both stoichiometric and air-diluted experiments, has proven to be an adequate procedure for analysing the combustion process in pre-chamber combustion systems. Using this methodology, the combustion features of the passive pre-chamber ignition concept fueled with different gasoline/hydrogen fuel blends have been evaluated in a lean environment ($\lambda = 1.9$).

The most relevant findings of this investigation are:

- The addition of hydrogen provides considerable benefits over the thermo-chemical properties of the mixture by increasing the laminar flame speed, reducing the flame thickness and improving the flame structure. This allows to achieve a stable combustion in both the pre-chamber and the main chamber volumes even at high diluted conditions ($\lambda = 1.9$).
- As the concentration of hydrogen in the mixture is increased, the temperature of unburned gases also rises, leading to a faster combustion into the main chamber. The resulting burning rate operating at $\lambda = 1.9$ is similar to that obtained at stoichiometric conditions with pure gasoline fuel, when adding 5% of hydrogen with respect to the intake volume fraction.
- The enhanced combustion process when considering 5% of H_2 addition at lean conditions ($\lambda = 1.9$) led to a significant efficiency gain of 3% in this particular engine architecture and operation condition.

- The rise of unburned gas temperature as the amount of H_2 increases, enhances the NO_x formation. Considering the smaller amount of hydrogen (2.5%), the NO_x emissions are significantly reduced, while maintaining suitable indicated efficiency levels (over 42%). This shows the potential of operating the engine at lean conditions without the use of the three-way catalyst.

This study provides interesting guidelines for improving the performance of modern SI engines by using hydrogen-enriched fuel blends in combination with a passive pre-chamber ignition system to enable lean combustion. In addition, this is a feasible short-term solution for passenger car aplications since no relevant engine modifications would be required. The conventional spark plug can be easily replaced by a passive pre-chamber system and there are several low-pressure hydrogen injectors for PFI available in the market. Therefore, integrating these technological bricks makes sense as a first step towards hydrogen economy and reducing CO_2 emissions from transportation.

Acknowledgements

The authors want to express their gratitude to CONVERGENT SCIENCE Inc. and Convergent Science GmbH for their kind support for the 0D, 1D and CFD calculations with the CONVERGE software.

Data Availability Statement

The data that support the findings of this study are available from the corresponding author upon reasonable request.

References

[1] J. Conti, P. Holtberg, J. Diefenderfer, A. LaRose, J. T. Turnure, L. Westfall, International energy outlook 2016 with projections to 2040, Tech. rep., USDOE Energy Information Administration (EIA), Washington, DC (United States ... (2016).

[2] N. Höhne, T. Kuramochi, C. Warnecke, F. Röser, H. Fekete, M. Hagemann, T. Day, R. Tewari, M. Kurdziel, S. Sterl, et al., The paris agreement: resolving the inconsistency between global goals and national contributions, Climate Policy 17 (1) (2017) 16–32.

[3] S. Jena, S. K. Kar, Setting a fostered energy network by decarbonizing the grid: Hybridization, control, and future solutions upon storage, International Journal of Energy Research 43 (1) (2019) 455–474.

[4] A. Chapman, K. Itaoka, K. Hirose, F. T. Davidson, K. Nagasawa, A. C. Lloyd, M. E. Webber, Z. Kurban, S. Managi, T. Tamaki, et al., A review of four case studies assessing the potential for hydrogen penetration of the future energy system, international journal of hydrogen energy (2019).

[5] M. Gurz, E. Baltacioglu, Y. Hames, K. Kaya, The meeting of hydrogen and automotive: a review, International Journal of Hydrogen Energy 42 (36) (2017) 23334–23346.

[6] P. Moriarty, D. Honnery, Prospects for hydrogen as a transport fuel, International Journal of Hydrogen Energy 44 (31) (2019) 16029–16037.

[7] S. E. Hosseini, M. A. Wahid, Hydrogen from solar energy, a clean energy carrier from a sustainable source of energy, International Journal of Energy Research 44 (6) (2020) 4110–4131.

[8] M. Ghazvini, M. Sadeghzadeh, M. H. Ahmadi, S. Moosavi, F. Pourfayaz, Geothermal energy use in hydrogen production: A review, International Journal of Energy Research 43 (14) (2019) 7823–7851.

[9] L. Das, Hydrogen engine: research and development (r&d) programmes in indian institute of technology (iit), delhi, International journal of hydrogen energy 27 (9) (2002) 953–965.

[10] J. Abe, E. Ajenifuja, O. Popoola, Hydrogen energy, economy and storage: review and recommendation, International Journal of Hydrogen Energy (2019).

[11] X. He, X. Hou, Q. Yang, X. Ma, G. Tian, F. Liu, Study of laminar combustion characteristics of gasoline surrogate fuel-hydrogen-air premixed flames, International Journal of Hydrogen Energy 44 (26) (2019) 13910–13922.

[12] S. Verma, A. Suman, L. Das, S. Kaushik, S. Tyagi, A renewable pathway towards increased utilization of hydrogen in diesel engines, International Journal of Hydrogen Energy 45 (8) (2020) 5577–5587.

[13] A. Vressner, P. Gabrielsson, I. Gekas, E. Senar-Serra, Meeting the euro vi nox emission legislation using a euro iv base engine and a scr/asc/doc/dpf configuration in the world harmonized transient cycle, Tech. rep., SAE Technical Paper (2010).

[14] A. J. Torregrosa, A. Broatch, J. García-Tíscar, J. Gomez-Soriano, Modal decomposition of the unsteady flow field in compression-ignited combustion chambers, Combustion and Flame 188 (2018) 469–482. doi:10.1016/j.combustflame.2017.10.007.

[15] M. Kowada, I. Azumagakito, T. Nagai, N. Iwai, R. Hiraoka, Study of Knocking Damage Indexing Based on Optical Measurement, SAE 2015 World Congress & Exhibition (2015). doi:10.4271/2015-01-0762.

[16] J. Wang, H. Chen, Z. Hu, M. Yao, Y. Li, A review on the pd-based three-way catalyst, Catalysis Reviews 57 (1) (2015) 79–144.

[17] G. Gonca, B. Sahin, Performance analysis of a novel eco-friendly internal combustion engine cycle, International Journal of Energy Research 43 (11) (2019) 5897–5911.

[18] N. Matulić, G. Radica, S. Nižetić, Thermodynamic analysis of active modular internal combustion engine concept: targeting efficiency increase and carbon dioxide emissions reduction of gasoline engines, International Journal of Energy Research 42 (9) (2018) 3017–3029.

[19] W. P. Attard, H. Blaxill, A lean burn gasoline fueled pre-chamber jet ignition combustion system achieving high efficiency and low nox at part load, Tech. rep., SAE Technical Paper (2012).

[20] D. Sarkar, Thermal power plant: design and operation, Elsevier, 2015.

[21] Y. Zeldovich, D. Frank-Kamenetskii, P. Sadovnikov, Oxidation of nitrogen in combustion, Publishing House of the Acad of Sciences of USSR, 1947.

[22] J. Li, H. Huang, N. Kobayashi, Z. He, Y. Nagai, Study on using hydrogen and ammonia as fuels: Combustion characteristics and nox formation, International journal of energy research 38 (9) (2014) 1214–1223.

[23] M. Ilbas, I. Yılmaz, T. N. Veziroglu, Y. Kaplan, Hydrogen as burner fuel: modelling of hydrogen–hydrocarbon composite fuel combustion and nox formation in a small burner, International journal of energy research 29 (11) (2005) 973–990.

[24] F. Hamori, H. C. Watson, Hydrogen assisted jet ignition for the hydrogen fuelled si engine, in: world hydrogen energy conference, no. 15, 2006.

[25] E. Toulson, H. C. Watson, W. P. Attard, The lean limit and emissions at near-idle for a gasoline haji system with alternative pre-chamber fuels, Tech. rep., SAE Technical Paper (2007).

[26] Z.-Y. Sun, Structure of turbulent rich hydrogen-air premixed flames, International Journal of Energy Research 42 (8) (2018) 2845–2858.

[27] H. Wu, L. Wang, X. Wang, B. Sun, Z. Zhao, C.-f. Lee, F. Liu, The effect of turbulent jet induced by pre-chamber sparkplug on combustion characteristics of hydrogen-air pre-mixture, International Journal of Hydrogen Energy 43 (16) (2018) 8116–8126.

[28] D. Nurmukan, T. J. M. Chen, Y. M. Hung, M.-Z. Ismadi, C. T. Chong, M.-V. Tran, Enhancement of biogas/air combustion by hydrogen addition at elevated temperatures, International Journal of Energy Research 44 (3) (2020) 1519–1534.

[29] S. Lee, S. Song, Hydrogen effects on ignition delay time of methyl butanoate in a rapid compression machine, International Journal of Energy Research (2020).

[30] Q.-h. Luo, J.-B. Hu, B.-g. Sun, F.-s. Liu, X. Wang, C. Li, L.-z. Bao, Experimental investigation of combustion characteristics and nox emission of a turbocharged hydrogen internal combustion engine, International Journal of Hydrogen Energy 44 (11) (2019) 5573–5584.

[31] E. Toulson, H. J. Schock, W. P. Attard, A review of pre-chamber initiated jet ignition combustion systems, Tech. rep., SAE Technical Paper (2010).
[32] S. Heyne, M. Meier, B. Imbert, D. Favrat, Experimental investigation of prechamber autoignition in a natural gas engine for cogeneration, Fuel 88 (3) (2009) 547 – 552. doi:https://doi.org/10.1016/j.fuel.2008.09.032.
URL http://www.sciencedirect.com/science/article/pii/S0016236108003712
[33] C. E. C. Alvarez, G. E. Couto, V. R. Roso, A. B. Thiriet, R. M. Valle, A review of prechamber ignition systems as lean combustion technology for si engines, Applied Thermal Engineering 128 (2018) 107–120.
[34] W. P. Attard, H. Blaxill, E. K. Anderson, P. Litke, Knock limit extension with a gasoline fueled pre-chamber jet igniter in a modern vehicle powertrain, SAE International Journal of Engines 5 (3) (2012) 1201–1215.
[35] M. Kettner, M. Rothe, A. Velji, U. Spicher, D. Kuhnert, R. Latsch, A new flame jet concept to improve the inflammation of lean burn mixtures in si engines, SAE transactions (2005) 1549–1557.
[36] J. Benajes, R. Novella, J. Gomez-Soriano, P. Martinez-Hernandiz, C. Libert, M. Dabiri, Evaluation of the passive pre-chamber ignition concept for future high compression ratio turbocharged spark-ignition engines, Applied Energy 248 (2019) 576–588.
[37] E. Toulson, H. C. Watson, W. P. Attard, Modeling alternative prechamber fuels in jet assisted ignition of gasoline and lpg, Tech. rep., SAE Technical Paper (2009).
[38] Z. H. Kyaw, H. C. Watson, Hydrogen assisted jet ignition for near elimination of nox and cyclic variability in the si engine, in: Symposium (International) on Combustion, Vol. 24, Elsevier, 1992, pp. 1449–1455.
[39] A. Boretti, H. Watson, A. Tempia, Computational analysis of the lean-burn direct-injection jet ignition hydrogen engine, Proceedings of the Institution of Mechanical Engineers, Part D: Journal of Automobile Engineering 224 (2) (2010) 261–269.
[40] G. Gentz, M. Gholamisheeri, E. Toulson, A study of a turbulent jet ignition system fueled with iso-octane: Pressure trace analysis and combustion visualization, Applied energy 189 (2017) 385–394.
[41] R. Novella, J. Pastor, J. Gomez-Soriano, I. Barbery, C. Libert, F. Rampanarivo, C. Panagiotis, M. Dabiri, Experimental and numerical analysis of passive pre-chamber ignition with egr and air dilution for future generation passenger car engines, Tech. rep., SAE Technical Paper (2020).
[42] F. Payri, S. Molina, J. Martín, O. Armas, Influence of measurement errors and estimated parameters on combustion diagnosis, Applied Thermal Engineering 26 (2) (2006) 226 – 236. doi:https://doi.org/10.1016/j.applthermaleng.2005.05.006.
URL http://www.sciencedirect.com/science/article/pii/S1359431105001560
[43] C. Guardiola, J. López, J. Martín, D. García-Sarmiento, Semiempirical in-cylinder pressure based model for nox prediction oriented to control applications, Applied Thermal Engineering 31 (16) (2011) 3275–3286.
[44] CONVERGENT SCIENCE Inc., CONVERGE 2.4 Theory Manual (2018).
[45] J. Benajes, R. Novella, J. Gomez-Soriano, I. Barbery, C. Libert, F. Rampanarivo, M. Dabiri, Computational assessment towards understanding the energy conversion and combustion process of lean mixtures in passive pre-chamber ignited engines, Applied Thermal Engineering 178 (2020) 115501.
[46] A. Torregrosa, P. Olmeda, B. Degraeuwe, M. Reyes, A concise wall temperature model for di diesel engines, Applied Thermal Engineering 26 (11-12) (2006) 1320–1327.
[47] F. E. Marble, J. E. Broadwell, The coherent flame model for turbulent chemical reactions, Tech. rep., PURDUE UNIV LAFAYETTE IN PROJECT SQUIDHEADQUARTERS (1977).
[48] T. Poinsot, D. Veynante, Theoretical and numerical combustion, RT Edwards, Inc., 2005.
[49] Y.-D. Liu, M. Jia, M.-Z. Xie, B. Pang, Enhancement on a skeletal kinetic model for primary reference fuel oxidation by using a semidecoupling methodology, Energy & Fuels 26 (12) (2012) 7069–7083.
[50] H. Wang, M. Yao, R. D. Reitz, Development of a reduced primary reference fuel mechanism for internal combustion engine combustion simulations, Energy & Fuels 27 (12) (2013) 7843–7853.
[51] L. Cai, H. Pitsch, Optimized chemical mechanism for combustion of gasoline surrogate fuels, Combustion and flame 162 (5) (2015) 1623–1637.
[52] M. Mehl, W. J. Pitz, C. K. Westbrook, H. J. Curran, Kinetic modeling of gasoline surrogate components and mixtures under engine conditions, Proceedings of the Combustion Institute 33 (1) (2011) 193–200.
[53] J. Brakora, R. D. Reitz, A comprehensive combustion model for biodiesel-fueled engine simulations, Tech. rep., SAE Technical Paper (2013).
[54] D. Davidson, B. Gauthier, R. Hanson, Shock tube ignition measurements of iso-octane/air and toluene/air at high pressures, Proceedings of the Combustion Institute 30 (1) (2005) 1175–1182.
[55] S. Jerzembeck, N. Peters, P. Pepiot-Desjardins, H. Pitsch, Laminar burning velocities at high pressure for primary reference fuels and gasoline: Experimental and numerical investigation, Combustion and Flame 156 (2) (2009) 292–301.
[56] C. Mandilas, M. Ormsby, C. Sheppard, R. Woolley, Effects of hydrogen addition on laminar and turbulent premixed methane and iso-octane–air flames, Proceedings of the combustion institute 31 (1) (2007) 1443–1450.
[57] S. Ravi, E. L. Petersen, Laminar flame speed correlations for pure-hydrogen and high-hydrogen content syngas blends with various diluents, International journal of hydrogen energy 37 (24) (2012) 19177–19189.
[58] T. Poinsot, D. C. Haworth, G. Bruneaux, Direct simulation and modeling of flame-wall interaction for premixed turbulent combustion, Combustion and flame 95 (1-2) (1993) 118–132.
[59] J. Benajes, R. Novella, J. Gomez-Soriano, P. Martinez-Hernandiz, C. Libert, M. Dabiri, Performance of the passive pre-chamber ignition concept in a spark-ignition engine for passenger car applications, in: SIA Power Train & Electronics, SIA Power Train & Electronics, Paris, France, 2019.
[60] R. Borghi, On the structure and morphology of turbulent premixed flames, in: Recent advances in the Aerospace Sciences, Springer, 1985, pp. 117–138.
[61] A. Broatch, P. Olmeda, X. Margot, J. Gómez-Soriano, Numerical simulations for evaluating the impact of advanced insulation coatings on h2 additivated gasoline lean combustion in a turbocharged spark-ignited engine, Applied Thermal Engineering 148 (2019) 674–683.

List of symbols/abbreviations

SI: Spark ignition. **CI**: Compression ignition. **TJI**: Turbulent jet ignition. **HAJI**: Hydrogen assisted jet ignition. **MC**: Main combustion chamber. **PC**: Pre-chamber. **ICE**: Internal combustion engine. **H_2 ICE**: Hydrogen Internal combustion engine. **CFD**: Computational fluid dynamics. **NO_x**: Nitrogen oxides. **H_2**: Hydrogen. **TWC**: Three-way catalyst. **PFI**: Port fuel injection. **DOHC**: Double over-head camshaft. **CO_2**: Carbon dioxide. **λ**: Relative air-to-fuel ratio. **RON95**: 95 Research Octane Number. **CCV**: cycle-to-cycle variability. **TDC**: Top dead center. **CAD**: Crank-angle degree. **HRR**: Heat release rate. **Δp**: Pressure difference between the pre-chamber and the main chamber. **CA50**: Combustion phasing. **IMEP**: Indicated mean effective pressure. **σIMEP**: Variability of the Indicated mean effective pressure. **MAPO**: Maximum Amplitude Pressure Oscillation. **MBT**: Maximum break torque. **ST**: Spark timing. **URANS**: Unsteady Reynolds-averaged Navier Stokes. **ECFM**: Extended Coherent Flamelet Model. **TKE**: Turbulent kinetic energy. **s_L**: Laminar flame speed. **l_f**: Flame thickness. **l_t**: Turbulence length scale. **u'**: Turbulent intensity.

List of Figures

List of Tables